Polym. Bull. (2011) 67:1671–1696
DOI 10.1007/s00289-011-0571-3

ORIGINAL PAPER

Strong thermoplastic elastomers created using nickel nanopowder

Witold Brostow · Martina Brozynski · Tea Datashvili · Oscar Olea-Mejía

Received: 15 February 2011 / Revised: 30 June 2011 / Accepted: 30 June 2011 /
Published online: 22 July 2011

Abstract We have decided to investigate whether addition of nickel (Ni) to a thermoplastic elastomer (TPE) will make TPE properties better for demanding applications. We have found that Ni particles moved well during low (100 °C) temperature blending, with the polymer providing more uniform particle dispersion. In contrast, at 160 °C, lower viscosity prevented particle dispersion and supported Ni agglomerations. All samples processed at low temperatures showed increased (by $\approx$10 °C) melting temperatures, higher crystallinity, and a 1.5 times higher Young's modulus E. While addition of Ni increases brittleness B of the blends, and so does vulcanization, a combination of both treatments lowers B. Some Ni particles go into existing free volume spaces in vulcanized materials thus enhancing mechanical properties including the storage modulus E'; some other filler particles create new free volume pockets increasing the elongation at break; thus, Ni particles at both kinds of locations provide lower values of brittleness. The addition of 0.5 wt% Ni particles to the uncured TPE matrix decreases the amount of extracted

W. Brostow (✉) · M. Brozynski · T. Datashvili
Laboratory of Advanced Polymers & Optimized Materials (LAPOM), Department of Materials Science and Engineering, Center for Advanced Research and Technology (CART), University of North Texas, 1150 Union Circle # 305310, Denton, TX 76203-5017, USA
e-mail: brostow@unt.edu
URL: http://www.unt.edu/LAPOM/

M. Brozynski
e-mail: mbrzynsk@yahoo.com

T. Datashvili
e-mail: tcd0033@unt.edu

O. Olea-Mejía
Centro Conjunto de Investigación en Química Sustentable, Facultad de Química, Universidad Autónoma del Estado de México, Toluca, Mexico 50120, Mexico
e-mail: oleaoscar@yahoo.com.mx

gel by 68.0 wt%. We used both Ni and oxidized Ni; they bestow similar properties on the TPE while providing stronger and less brittle materials than neat TPE.

Keywords Thermoplastic elastomer · Nickel filler · Brittleness · Oxidation · Nanocomposite

Introduction

Modern technology continuously needs new materials with special combinations of properties. The advances in technology are connected to a widening application of engineering polymeric materials (engineering plastics) in the automotive, aviation, construction and petroleum industries, manufacture of consumer goods, and medicine [1–4].

Strength, lighter weight, versatility, ease of processing, and low cost have been the motives to replace traditional metals and ceramics with polymer-based materials (PBMs). Unlike metals or ceramics, PBMs allow to lower the weight and to increase the output of parts—along with increase resistance to chemically hostile conditions. The ability to tailor structure—by adding fillers [5–21] and thus affecting the strength/stiffness when required—means that polymer composite structures can be more efficient and effective than other materials. In recent years, polymer nanocomposites (PNCs) have become more and more attractive [6, 9, 22–28]. Embedded nanoparticles can profoundly affects important properties of the polymers and thus enlarge the range of potential applications of polymers. Through control or alteration of the additives at the nanoscale level, one is able to enhance the properties of selected polymer systems to meet or exceed the requirements of current military, aerospace, and commercial applications [29].

Thermoplastic elastomers (TPEs) are an important class of polymers. Car tires, rubber bands, and many other products are made from elastomers—that is, polymeric materials in which lack of rigidity is the main advantage. TPE-based nanocomposites containing clay have been studied in some detail. Thus, Naderi et al. [30] investigated materials containing polypropylene (PP), ethylene-propylene-diene rubber (EPDM), a clay, and a compatibilizer. They have found differences in properties between materials prepared with low viscosity PP or else with high viscosity PP. Ho et al. [31] developed a novel class of insulating materials using thermoplastic polyurethane elastomers (TPUs) filled with nanoclays and carbon nanofibers. We recall that PUs have a large variety of structures [32–34]. The nanofillers most often used in plastics are carbon nanomaterials (including fullerene or its derivatives) [7, 22] or layered clay minerals [9, 16]; ceramic particles have also been used [26]. Like ceramic or carbon-filled polymers, metal-filled PNCs have the potential to combine both performance and processability [35–37].

Given the advantages of elastomers noted above and a very large amount of elastomers produced annually [38, 39], we have decided to synthesize dynamic vulcanized blends of PP and EPDM [40, 41] filled with 0.5 wt% nickel nanoparticles. We have studied before [35] properties of hybrids containing low density polyethylene (LDPE) and in turn Ag, Al, and Ni. Values of dynamic friction

of the hybrids against polytetrafluoroethylene (PTFE) show that addition of Ni to LDPE results in instantaneous lowering of the friction; for the other two metals, there are maxima on the dynamic friction versus metal concentration diagrams. We expected that nano-sized nickel might significantly change the properties of the thermoplastic vulcanized elastomer (TPV) products. Furthermore, TPV-based nanocomposites are good candidates for the development of new types of lightweight and high-performance solar absorbing roofing laminates for increased solar energy conversion. Moreover, a combination of nickel particles with TPV matrix is one way to stabilize the Ni particle to avoid problems of oxidation and lower the danger of corrosion. In order to evaluate the effects of nickel nanopowder on thermal and mechanical behavior of TPV composites, we have taken into account extant results of studies on oxidation of nickel nanoparticles [42–44]. The sample size dispersion and elemental composition of the nickel powder before and after oxidation were characterized using transmission electron microscopy (TEM), energy dispersive X-ray spectroscopy (EDS), and thermogravimetric analysis (TGA). For TPV + nickel and TPV + oxidized nickel nanocomposites, we have studied relationships between the glass transition temperature T_g, crystallinity, swelling, morphology, and mechanical properties. The experiments for uncrosslinked EPDM + PP + 0.5 wt% Ni blends were performed and compared with those of the crosslinked composites. In order to achieve homogenous dispersion of nanopowder inside TPV matrix, two different techniques were pursued. Composites were prepared using nickel powder (Method 1—loading temperature 160 °C) and nickel powder suspension in methanol (Method 2—loading temperature 100 °C), as detailed below.

Experimental part

Materials

Ethylene-propylene-diene rubber and modified metallic diacrylate co-agent (SR633) were received as a gift from Dow Chemical Company and Sartomer Company, Inc., respectively. PP pellets were supplied by Huntsman Co. Table 1 lists some properties of the polymers used.

A silane coupling agent (SCA) namely vinyltrimethoxysilane (VTMOS) was received as a gift from Struktol Company of America. Dycumyl peroxide (DCP),

Table 1 Properties of the polymers

Material	PP	EPDM
23 °C density/(g cm^{-3})	0.917	0.882
Mooney viscosity/ML 1 + 4 at 125 °C	–	25
Degree of crystallinity/vol.%	39.7	0.0
Molecular weight	232.000	135.000
Ethylidenenorbornene content/mass%	–	4.9

methanol, cyclohexane, and nickel powder were from Sigma Chemicals Co. The reagents were analytically pure and were used as-received.

Characterization techniques

Differential scanning calorimetry (DSC)

The DSC technique is well described by Lucas and her colleagues [45], Menard [46], and Gedde [47]. DSC measurements were performed on a Perkin Elmer (DSC-7) instrument. The temperature range from 0 to 200 °C was covered under a nitrogen atmosphere at 10 °C/min heating and cooling rates. The melting temperatures T_m, crystallization temperature T_c, and enthalpies of fusion H^f were obtained by analyzing the DSC thermograms. Volumetric degree of the crystallinity X_c was calculated as

$$X_c[\%] = 100\, H^f / H^f_{PP}. \quad (1)$$

Here $H^f_{PP} = 209$ J/g is the enthalpy of fusion of extrapolated 100% crystalline PP [47, 48].

Dynamic mechanical analysis (DMA)

The tests were carried out using a DMA7e apparatus from Perkin Elmer Co. The DMA technique has also been described by the same authors [45–47]. Specimens were analyzed in rectangular form using the three point bending fixture in the temperature scan mode at the heating rate of 5 °C/min. The frequency applied was 1.0 Hz. We registered the storage (solid-like) modulus E', the loss (liquid-like) modulus E'', and tan δ as a function of temperature

$$\tan \delta = E''/E'. \quad (2)$$

Thermogravimetric analysis (TGA)

A Perkin Elmer TG-7 instrument was used to determine a temperature profile of the powder. Five milligrams of each dried sample was placed on a balance and heated over the temperature range from +50 to 700 °C at the heating rate of 10 °C/min.

Environmental scanning electron microscopy (ESEM) and energy dispersive spectroscopy (EDS)

Energy dispersive spectroscopy of all powder samples were taken using a FEI Quanta Environmental Scanning Electronic Microscope (ESEM) configured with EDS.

Transmission electron microscopy (TEM)

The particles before and after oxidation were characterized under a JEOL 2100 TEM at 200 kV of acceleration voltage to determine their shape and size distribution.

Focused ion beam/scanning electron microscope (FIB/SEM)

The FEI Nova 200 NanoLab [a dual column ultra high-resolution field emission scanning electron microscope (SEM) and focused ion beam (FIB)] were used to study the morphology of the composites [37]. In this technique, we use both beams (electrons and ions) without removing the sample from the analysis chamber. First, an area for milling is selected with the electron beam, and then the milling is made with the Ga^+ ion beam. The two beams are at 52° from each other; this allows observing one side of the milled parallelepiped with the electron beam. The composites were milled with 0.5 nA Ga^+ ion beam current at an accelerating voltage of 30 kV. The observed inner region of the cross-sectional area was polished (cleaned) with the same beam current 0.5 nA.

A small fraction of the samples was mounted on a copper stub and coated with a thin layer of gold and palladium to avoid electrostatic charging during examination.

Tensile testing

The static tensile behavior of the samples was determined at room temperature with a MTS tester (model QTEST/5) according to ASTM D-638. The tests were performed in a controlled environment in order to determine the elongation at break, strain at break, and modulus. The cross-head speed was 100 mm/min; five specimens of each sample were tested and average values are reported.

Gel content

Rectangular sample pieces with dimensions 15 × 7 × 2 mm^3 were used for testing. Cyclohexane was used to immerse the samples at 23 °C in the liquid. After 24 h, the cyclohexane was refreshed to remove the extracted components. After another 24 h, the swollen samples were weighted, dried, and weighed again. The drying of the samples was performed at 50 °C for 48 h in order to remove the solvent. Swelling behavior is related to the bulk modulus (the reciprocal of isothermal compressibility) and also to diffusivity [49]. The relative gel content m_g with respect to the initial mass m_0 was calculated from the difference between m_0 and m_d, where m_d is the mass after drying the sample. The gel amount in the composites was determined as:

$$\text{gel}(\%) = \frac{m_0 - m_d}{m_0} 100\%. \quad (3)$$

Oxidation and modification of nickel powder

Nickel powder was oxidized for a period of 19 h in a Burnsted Thermolyne furnace at a constant temperature of 400 °C. The initial nickel powder, after oxidation, gained approximately 22 wt%.

Chemical treatment of nickel powder was performed using a vinyltrimethoxysilane (VTMOS) and a suspension of aluminum oxyhydroxide (AlOOH). A typical example can be described as follows. The reaction mixture contained 3.0 g VTMOS, 3.0 g of methanol, and 20 g ≈ 3.0 wt% AlOOH (Boehmite) suspension

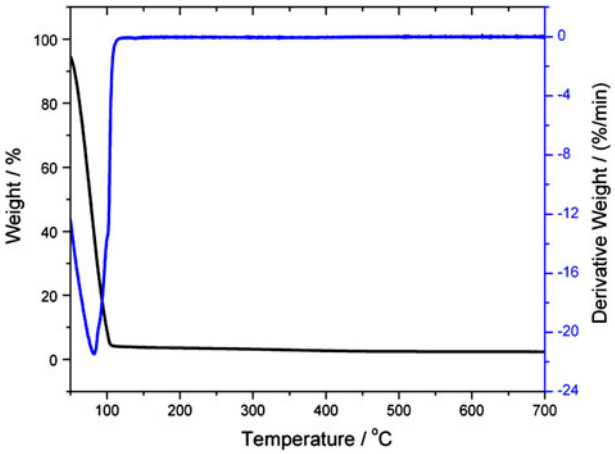

Fig. 1 TGA diagram: boehmite suspension in methanol

in methanol. 2.0 g of nickel powder was added slowly under thorough stirring of the mixture. After another 3 h of stirring, the resulting mixture was refluxed at 70 °C for 2 h. The final product was collected by centrifugation, washed with fresh methanol, and then vacuum dried for 24 h at 110 °C. The classic Yoldas process [50] was used to prepare the AlOOH (Boehmite) suspension in methanol (Fig. 1).

Aluminum isopropoxide ($Al(OC_3H_7)_3$) from Sigma-Aldrich was chosen to be the precursor of Boehmite. In order to achieve complete hydrolysis, the molar ratio of aluminum isopropoxide to water was kept 1:150. Hydrolysis occurs according to the reaction:

$$2\left(Al(CH_3)_2CHO\right)]_3 + (3 + n)H_2O \rightarrow Al_2O_3 \cdot nH_2O + 6(CH_3)_2CHOH.$$

During the subsequent evaporation of approximately half the amount of H_2O under constant stirring, HNO_3 is added in order to clear the solution and to maximize the Al content at the gelling point. After cooling down to room temperature, a clear gel is obtained. This gel is then mixed with an appropriate amount of methanol to obtain $\approx$3.0 wt% Boehmite suspension in CH_3OH (Fig. 1). Thus, Ni particles are coated with Boehmite gel so that hydroxide groups of Boehmite facilitate grafting. VTMOS has two types of reactive groups. One of the groups (methoxysilane) reacts with inorganic constituents, while the other one (vinyl) reacts with organic constituents present.

Sample preparation

The composites were prepared by melt mixing in a C.W. Brabender D-52 Preparation Station. EPDM was added first and softened at 160 °C (Method 1) and/or at 100 °C (Method 2) with a blade rotation speed of 60 rpm during 2 min, followed by the addition of 0.5 wt% nickel powder (Method 1) and/or 0.5 wt% nickel powder suspension in methanol (Method 2). After 2 min of mixing, PP was

added. Immediately afterward, 1.0 wt% of the curing agent (DCP) and 0.5 wt% of SR633 (for minimizing the PP degradation) were added, and temperature and mixing speed were increased and kept for 2 min at 190 °C and 90 rpm. The amount of peroxide was calculated on the basis of EPDM + PP weight.

The resulting samples were pelletized, and the blends were then molded in an AB-100 injection machine (AB Machinery, Montreal, QC, Canada) at 175 °C with an injection pressure of 830 kPa.

Characterization of nickel particles

The particles before and after oxidation were characterized with a TEM in order to determine their shape and size distribution. TEM images are shown in Fig. 2.

Nickel particles are approximately spherical with a wide diameter distribution between 10 and 120 nm. The average particle size estimated from TEM images is 41.5 nm, which is higher than an average particle size of 28.0 nm stated by the provider. As oxygen is incorporated via oxidation of Ni particles, they tend to grow in size. The particle shape becomes irregular after oxidation (Fig. 2b). The particles are in the form of aggregates or even sintered clusters—an implication of melting occurring during the oxidation experiments. The average size of oxidized Ni particles is 45.3 nm. Song et al. have reported that oxidation of Ni nanoparticles is accompanied by early melting, far below nickel's bulk melting temperature $T_m \approx 1450$ °C [42].

When the particles are modified, their size remains practically the same, namely 45.5 nm, see Fig. 2c. It is important to note that the oxidized and modified particles are better dispersed than untreated Ni, as seen in the TEM images. The particle size histograms are shown in Fig. 3.

In order to quantitatively investigate the oxidation behavior, the elemental composition of nickel nanoparticles (as-received) and particles after oxidation and modification experiments were analyzed by energy dispersive EDS (Fig. 4).

The EDS results confirm the high purity of nickel particles; ≈99.9 wt% of the metallic components is nickel, which is consistent with the data from the manufacturer. The EDS analysis also identified the presence of 0.4–1.3 wt% oxygen at different scanned areas of the nickel particles prior to the oxidation experiments. This implies that different levels of initial oxidation of nickel particles occurred during the production or storage period. This might be caused by a non-uniform distribution of defects in nickel crystal structures, i.e., areas with large defects could cause high oxidation levels and vice versa. Statistical oxygen weight concentration in these five areas was 0.85 wt%; this equals a nickel oxide concentration of 3.96% by weight. EDS also shows us a high degree of oxidation for the nickel nanopowder and the signs of the Ni powder treatment. Identified Si and Al peaks are the evidence of the modification progress (Fig. 4c).

Diffraction patterns of Ni particles were recorded using the TEM diffraction mode to study the crystallography of the samples (Fig. 5).

As expected, Ni nanoparticles have a face-centered cubic (FCC) crystal structure, the same as the metallic Ni (Fig. 5). In the diffraction pattern of oxidized Ni

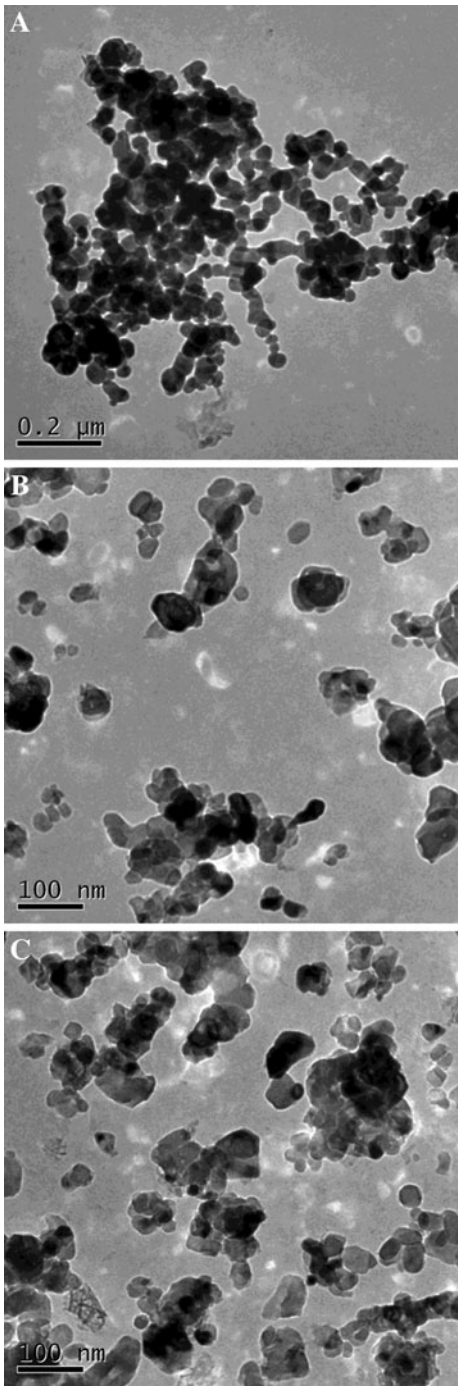

Fig. 2 TEM images: Ni (**a**), oxidized Ni (**b**), and oxidized/modified Ni–O–M (**c**)

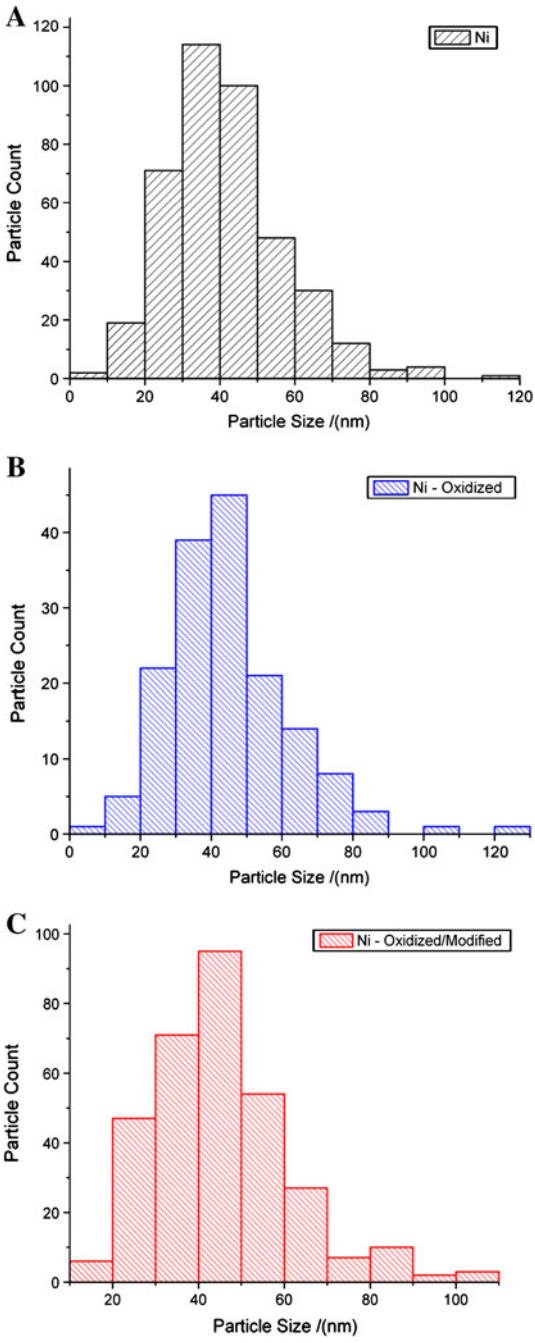

Fig. 3 The particle size histograms: Ni (**a**), oxidized Ni (**b**), and oxidized/modified Ni–O–M (**c**)

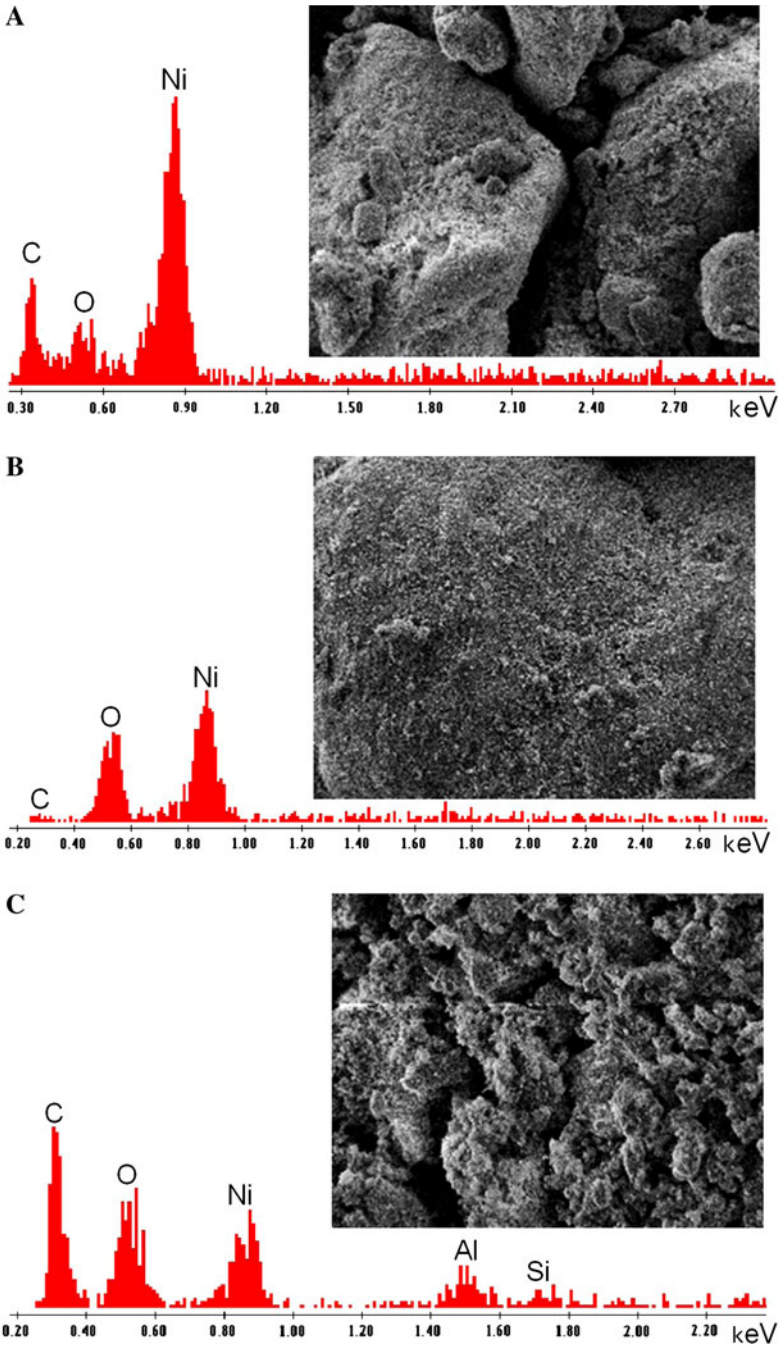

Fig. 4 EDS: Ni (**a**), oxidized Ni (**b**), and oxidized/modified Ni–O–M (**c**)

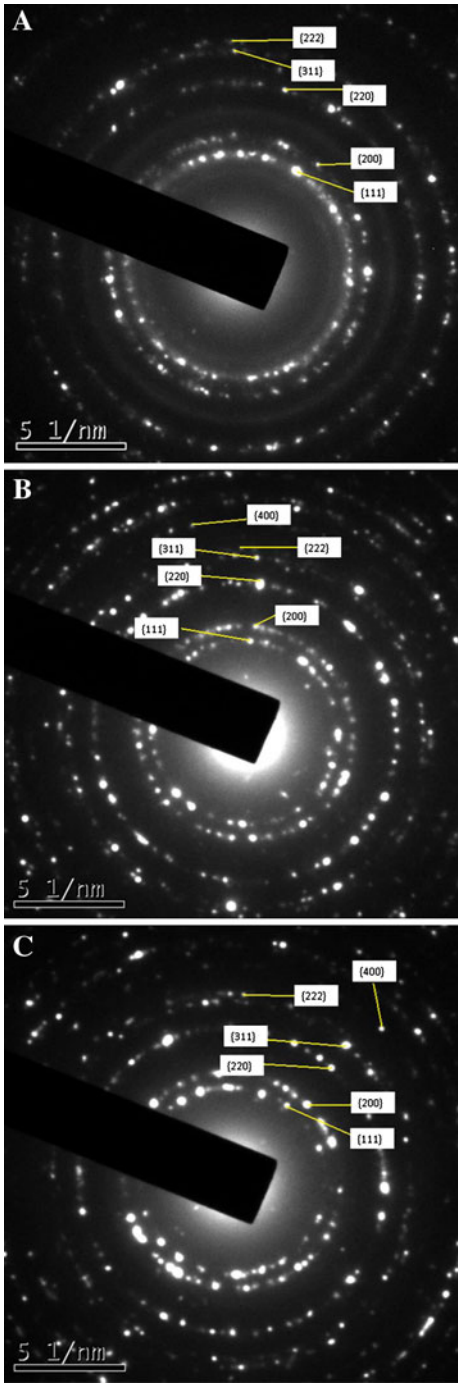

Fig. 5 Diffraction patterns: Ni (**a**), oxidized Ni (**b**), and oxidized/modified Ni–O–M (**c**)

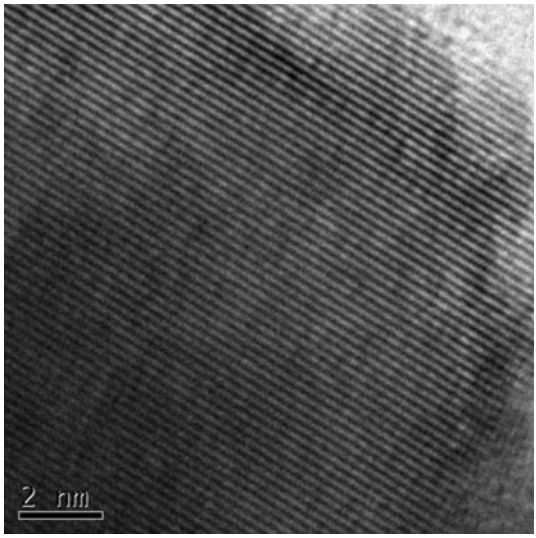

Fig. 6 HRTEM image of single oxidized Ni particle

nanoparticles, we observe NiO phase (an FCC rock salt structure). The rings here are smaller and they correspond to larger distance between the planes (the lattice parameter of Ni is 0.352 nm, while for NiO it is 0. 41 nm).

From the high-resolution TEM (HRTEM) image of a Ni nanoparticle, we determined a planar distance of 0.23 nm that corresponds to the planes {111} of NiO with the lattice parameter of 0.41 nm (Fig. 6).

Finally, for the modified Ni particles, we observe the same crystalline structure as for the oxidized particles.

Thermogravimetric analysis was chosen to evaluate the oxidation process. TGA diagrams of the samples (Ni, oxidized Ni, and oxidized/modified Ni) are shown in Fig. 7.

Thermograms of the modified samples show two regions of characteristic weight loss at $\approx$100 and 250 °C. This can be explained by absorbed residues such as water and solvent as well as by the decomposition of the organic constituent of the grafted VTMOS. The weight of the oxidized powder remains constant; we infer that Ni nanoparticles were fully oxidized. Significant differences in thermal behavior between the unoxidized and oxidized samples are associated with the oxidation reaction. The Ni nanoparticles begin to show a gain in weight at 200 °C in the thermogravimetric curve, suggesting that oxidation occurs at this temperature. Compared to the typical initial oxidation temperature of bulk nickel materials, $\approx$600 °C, the oxidation of nanoparticles occurs at a much lower temperature. A pronounced change in oxidation kinetics occurs around 490 °C—as observed from the slope decrease of the TGA curve. The decreased oxidation rate extends toward higher temperatures before approaching an asymptotically constant value: an indication of full oxidation of the specimen. The final weight increase of this sample material is 20.8%, which is somewhat lower than the ideal weight increase of 27.3% for a completely pure nickel oxidation. As observed from the EDS analysis, typical

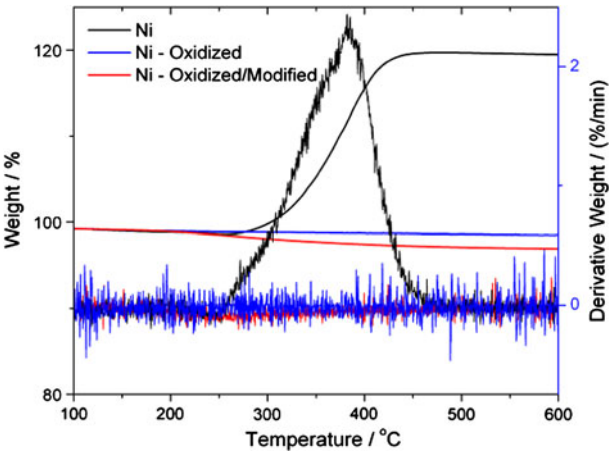

Fig. 7 TGA scans and derivative curves for the powder

nanoparticle samples contain some initial oxides, presumably a thin layer of amorphous oxide.

Dispersion of nickel particles

One of the main objects of our work was evaluation of effects of nickel particles dispersion on the overall material properties. Thermal and mechanical characteristics depend to a great extent on the matrix–filler interactions at the molecular scale; as noted by Kopczynska and Ehrenstein, properties of multiphase composites are to a large extent decided by interfaces [51].

Since a homogeneous dispersion of nickel nanoparticles would be a key factor to improve the properties of the TPV composites, we decided to investigate the Ni particles dispersion inside the polymer matrix using the FIB/SEM method [37]. This technique combines a scanning Ga^+ focused ion beam (FIB) column with high-resolution field emission scanning electron microscope (FESEM). FIB/SEM images of the composites are presented in Fig. 8.

We recall that for controlling Ni nanoparticles dispersion in the TPV matrix, we used two different blending temperatures. Moreover, in Method 1 (160 °C) we used dry Ni powder, while in Method 2 (100 °C) we had Ni suspension in CH_3OH.

It can be seen from SEM images that morphology of the samples from Method 1 and Method 2 are very different. The first approach did not seem to ensure uniform dispersion of isolated nanoparticles. From the SEM images, we can see agglomeration of Ni particles and formation of $\approx$250 nm size clusters for the most of the samples. However, more uniform particle dispersion was noticed inside the unvulcanized EPDM + PP matrix compared to other samples from the same group in Method 1 (Fig. 9a). The particle agglomerations and formation of Ni clusters can be observed even for this sample but they are homogeneously distributed inside the unvulcanized specimen. For the vulcanized composites (Method 1), it was

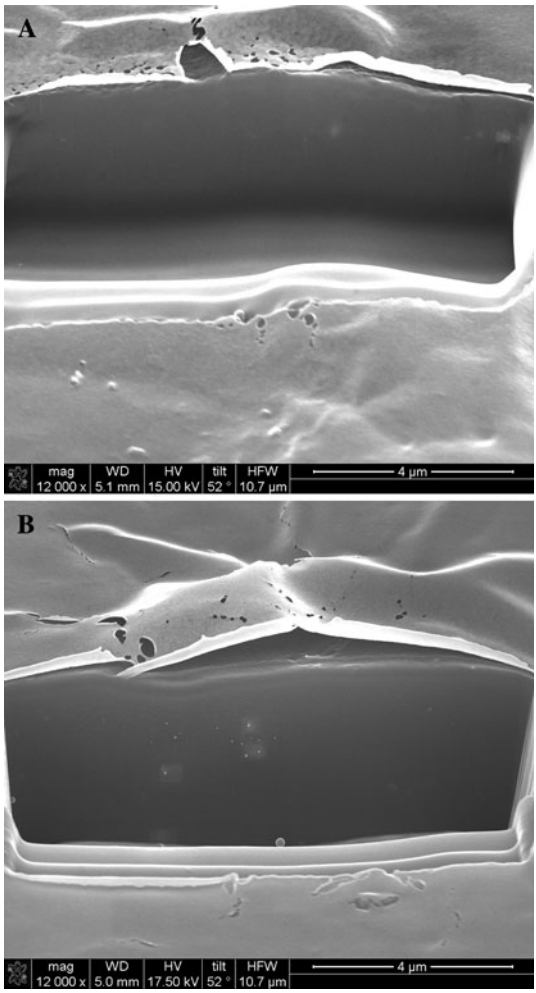

Fig. 8 FIB/SEM images of the composites from Method 1 (**a**) and Method 2 (**b**): PP/EPDM + 0.5 wt% Ni (**a**), PP/EPDM + 0.5 wt% Ni (CH_3OH) (**b**)

challenging to locate particles inside the milled segment; when we found one, it was a big cluster of the Ni particles. It needs to be noted that the volume of milled material (10 × 5 × 5 μm) was kept constant for all the samples.

Let us return to the samples from Method 2. Particle dispersion in the TPV matrix became uniform when filler was added into the molten phase of the EPDM at lower temperature (100 °C). This fact could be explained by the viscosity of the EPDM matrix. From the FIB/SEM images of frozen structures, it can be clearly observed that Ni particles have dispersed better in a more viscous EPDM matrix (lower *T*), while lower viscosity (higher *T*) prevents particle detachment and dispersion—resulting in an obstacle against their uniform distribution. All the samples from Method 2 show better particle dispersion compared to the same samples from Method 1. For the vulcanized samples, it is hard to see that we obtained samples

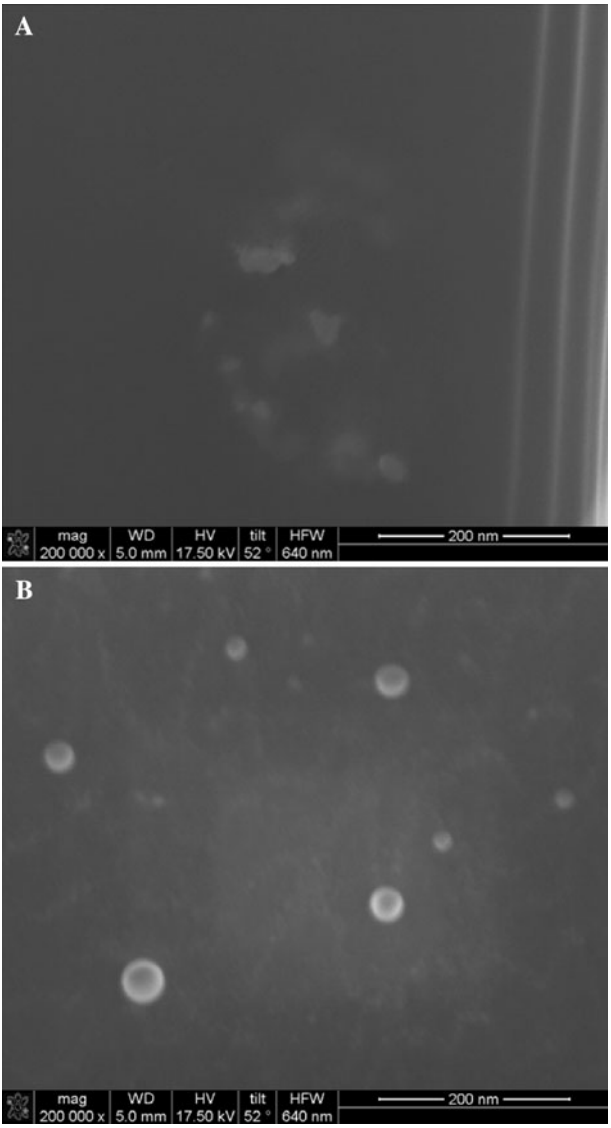

Fig. 9 FIB/SEM images of the composites from Method 1 (**a**) and Method 2 (**b**): PP/EPDM + 0.5 wt% Ni (**a**), PP/EPDM + 0.5 wt% Ni (CH_3OH) (**b**)

where individual $\approx$45 nm size particles are interacting with TPV matrix but still significant improvement was observed.

It was nice to see perfectly dispersed particles inside unvulcanized matrix from Method 2. In Fig. 9b, we see a homogeneous individual particle dispersion inside PP + EPDM matrix.

We plan to do more work to understand the role of viscosity (or rheology and processing conditions in general) on the nanoparticles dispersion in a various

polymeric phases. There might be other factors affecting particle dispersion; free volume has been already noted in a different context. The decrease of the free volume during vulcanization might prevent particle detachment and promote formation of clusters.

Thermal and mechanical properties and gel content

The DMA and DSC techniques have been used to study the components miscibility and to determine the effects of the blend composition and Ni particles dispersion on the properties of our TPV + Ni hybrids.

EPDM + PP and their composites were subjected to a controlled sinusoidal oscillation force, and the resultant mechanical response was measured. The storage modulus E', loss modulus E'', and mechanical loss factor (tan δ) curves versus temperature for 1.0 Hz are presented in Fig. 10a–c (symbols and colors are the same in all figures).

Two separate transitions from a glassy to a rubbery state are visible in the temperature range from −50 to +40 °C, corresponding to relaxations of the individual components. Two distinct peaks indicate the immiscibility of the EPDM and PP components. After vulcanization of PP with EPDM, the storage and loss moduli of the system went down while tan δ increased. The temperature at which tan δ rapidly increases shifted upwards after curing. This indicates that the EPDM was crosslinked and the interaction between the EPDM and PP has improved.

EPDM + PP matrix displays well-known behavior characteristic for immiscible thermoplastic + elastomer blends. Below T_g, both polymers are in the glassy state with a roughly constant modulus. After T_g is reached, a strong decrease in E' can be noticed. DMA experiment with 3-point bending fixture fails above T_g due to the bending of the specimen. By definition, above T_g the material is in the rubbery state until the material starts to flow; then it behaves as a viscous fluid. In this respect, DMA technique was helpful to understand the performance of each material in the glass transition region.

As shown in Fig. 10a, all the composites from Method 2 and uncrosslinked PP + EPDM composite from Method 1 maintain higher value of E' above T_g of PP. Furthermore, the temperature range in which creep deformation occurred is increased up to 25 °C for all nanocomposites from Method 2. This phenomenon is due to the formation of a connective network of Ni particles within the polymer matrix. The entanglement level of this network and the interactions between the polymer chains and the nanoparticle surfaces can explain the delay of the material flowing and the existence of such a wide modulus plateau. Overall, the highest value of E' above T_g of PP is seen for unvulcanized PP + EPDM + 0.5 wt% Ni sample from Method 2. For instance, at 40.0 °C, the E' of this material is 1.6 times higher than that of the unfilled PP + EPDM and 1.3 times higher than for the same composition from Method 1.

As discussed in "Dispersion of nickel particles" section, filler agglomeration and inhomogeneous dispersion were seen for the composites prepared via Method 1.

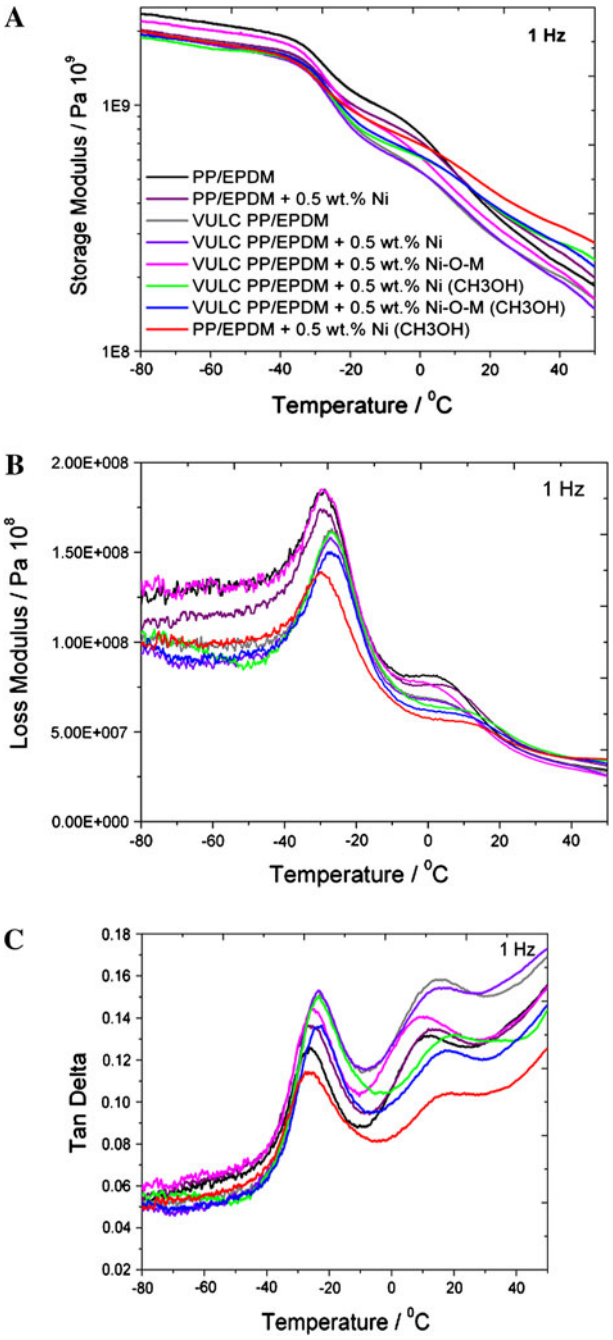

Fig. 10 DMA diagrams: storage modulus E' (**a**), loss modulus E'' (**b**), and tan δ (**c**)

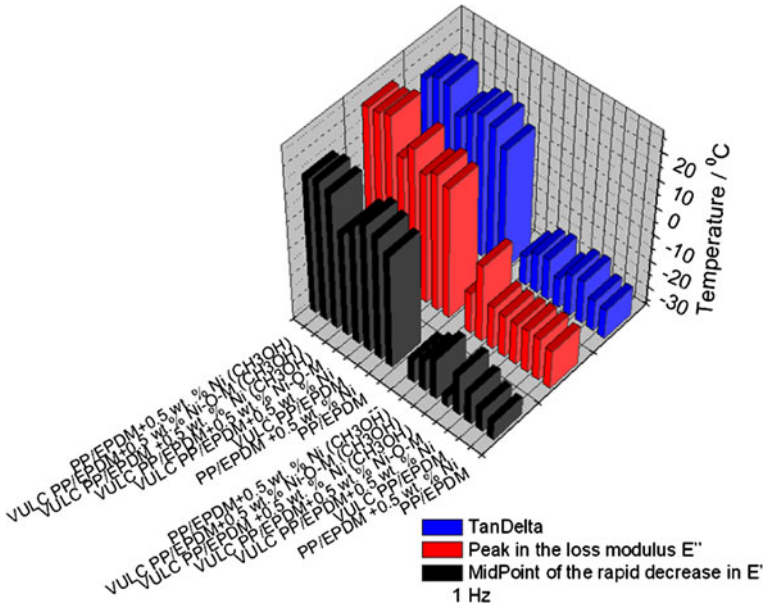

Fig. 11 Glass transition temperatures from DMA

Particles agglomeration decreases material performance because of formation of voids that act as preferential sites for crack initiation and failure [36].

In terms of thermophysical properties, T_g is one of the most important and useful material characteristics. Glass transition temperature can be used to determine a material's maximum temperature of use. For both fundamental and practical reasons, it was recommended [52] to define the glass transition temperature (T_g) as the midpoint of the rapid decrease in the storage modulus E'. Since glass transition is so important, we used a peak in the loss modulus E'', a peak in tan δ as well as the midpoint of the rapid decrease in the storage modulus E' to evaluate effects of Ni on the T_g values of PP and EPDM (Fig. 11).

Among the three methods used, two have shown good and mutually consistent results. Broad peaks in the loss modulus E'' did not lend themselves to provide accurate locations of the glass transitions.

Let us return to analyze the effect of Ni content on the transitions. Figure 11 tells us that T_g values of PP go up in the presence of Ni. The effect is larger when Ni particles are incorporated at lower temperature in the form of suspension in CH_3OH (Method 2). In the same manner, it can be observed that the T_g of PP in vulcanized PP + EPDM system shifted toward higher temperatures. On the other hand, loading Ni powder at a high temperature (Method 1) in vulcanized matrix of PP + EPDM gives rise to a displacement of the T_g peak of PP to *lower* temperatures. This effect was more evident when oxidized + modified Ni powder is incorporated at high temperature to the vulcanized PP/EPDM system. These results seem to indicate that during high-temperature blending the chemical (VTMOS) groups of the treated Ni powder surface underwent decomposition—in turn causing creation of shorter

chains by scission. The scission apparently overwhelmed the crosslinking process; hence, lower T_g values of the polymers.

Since mechanical properties of semicrystalline polymers are influenced by their crystalline structures, it is pertinent to determine effects of Ni content on thermophysical properties of the composites. Melting temperatures (T_m), crystallization temperatures (T_c), heats of fusion (H_f), and the percentages of crystallinity (X_c) were determined in non-isothermal crystallization experiments. The results are reported in Table 2.

Dynamic crystallization behavior shows the positive effect of the Ni content on the crystallization kinetics of PP. DSC data confirmed earlier observation [40] about nucleation ability of cured EPDM. Compared to the neat PP + EPDM blend, higher crystallization temperatures were found for all vulcanized PP/EPDM samples and composites. This phenomenon can be explained by an interaction of the amorphous portion of the PP with the EPDM. Moreover, a marked increase of the crystallization peak temperature can be observed when Ni particles are incorporated in the PP + EPDM matrix at the lower temperature (Method 2). This effect is more pronounced when the fillers are oxidized and chemically treated. The results can be explained by a nucleation ability of the well-dispersed Ni and Ni–O–M particles on the PP crystallization.

From DSC results, it can be easily noticed that the nanoparticles dispersion was a key factor to determine the materials thermal properties. Namely, PP/EPDM + 0.5 wt% Ni sample from Method 2 was not even crosslinked; however, compared to other crosslinked or blended samples from Method 1, it showed higher crystallization and melting point. These results are in an agreement with those obtained in a morphological study where improved nonoparticles dispersion was demonstrated by the samples from Method 2. Furthermore, the melting temperature of the PP phase increased by about 10 °C for the composites from Method 2, while no changes in the melting point were detected in the samples from Method 1.

As shown in Table 2, values of the crystallinity decrease with the crosslinking. This can be understood as a result of decreased PP chain mobility due to crosslinking and increased viscosity of the blends caused by the curing agent. In addition, we did not observe any remarkable effect of the Ni content on the

Table 2 Thermal properties of the materials

Sample name	T_c/°C	H_c^f/J g^{-1}	X_c/%	T_m/°C	H_m^f/J g^{-1}	X_c/%
PP/EPDM	84.9	37.9	18.1	143.7	32.0	15.3
PP/EPDM + 0.5 wt% Ni	86.6	34.5	16.5	143.7	12.6	6.0
VULC PP/EPDM	92.6	29.5	14.1	142.3	12.7	6.1
VULC PP/EPDM + 0.5 wt% Ni	92.3	31.8	15.2	141.3	11.3	5.4
VULC PP/EPDM + 0.5 wt% Ni–O–M	91.6	39.2	18.7	142.3	13.4	6.4
VULC PP/EPDM + 0.5 wt% Ni (CH_3OH)	102.6	35.5	17.0	154.7	19.6	9.4
VULC PP/EPDM + 0.5 wt% Ni–O–M (CH_3OH)	103.6	40.8	19.5	152.7	26.8	12.8
PP/EPDM + 0.5 wt% Ni (CH_3OH)	99.9	42.6	20.4	159.3	25.9	12.4

crystallinity of the crosslinked composites from Method 1. All these samples maintained a crystallinity value similar to the unfilled and crosslinked PP + EPDM sample. However, the same composites from Method 2 showed a somewhat higher crystallization degree of the PP phase. In fact, it can be noticed that two uncured PP/EPDM blends with 0.5 wt% Ni (from Methods 1 and 2) filler gave completely different values of the crystallinity. Decreased crystallization of the PP/EPDM + 0.5 wt% Ni sample (Method 1) was directly associated with the dilution effect of the agglomerated Ni particles.

We now return to the strain at break ϵ_b which is an important parameter and appears in the definition of material brittleness B [53]; see more on B below. Young's modulus E and the strain-at-break values obtained from tensile testing are summarized in Fig. 12a and b.

Compared to uncured blends, lower moduli E can be seen for all cured composites. Young modulus value for the vulcanized PP + EPDM blend is about 2.2 times lower than for unvulcanized PP + EPDM blend. However, the samples prepared using DCP as the curing agent provide higher values of ϵ_b relative to the uncured PP + EPDM blends. Clearly, crosslinked compositions should be considered as thermoplastic rubbers more than as a toughened thermoplastic. Uncrosslinked samples exhibit definite plastic behavior and high Young's moduli.

The increase in the modulus after filler loading in vulcanized PP + EPDM blend shows the same trend as observed from the DMA storage modulus curves. Young modulus E values of the VULC PP + EPDM + 0.5 wt% Ni and VULC PP + EPDM + 0.5 wt% Ni–O–M composites from Method 1 are about 1.2 and 1.4 times higher than E value of the vulcanized PP + EPDM. Higher modulus E values are seen for all the composites. However, vulcanized Ni composites prepared via Method 2 displayed the highest modulus. Moreover, any given oxidized/modified Ni containing sample (Method 2) had the highest modulus increment, equal to 195.0 MPa. It can be seen clearly that the treatment of the nickel powder induced the enhancement of tensile strength from 298 MPa of VULC PP + EPDM to 403 and 493 MPa for VULC PP + EPDM + 0.5 wt% Ni–O–M composite from Method 1 and Method 2, respectively. These results can be explained by improved adhesion between the filler and the polymer interfaces. The strain at break ϵ_b value of the vulcanized PP + EPDM sample increases with Ni content (Fig. 12b). This can be explained by new free volume pockets in the material created by the Ni particles added. Brittleness B of materials is defined [53] as

$$B = 1/\left[E'\epsilon_b\right] \tag{4}$$

Here E' pertains to the frequency of 1.0 Hz and the temperature of interest, in the present case 25 °C. Thus, B takes into account repetitive loading (fatigue in service) as well as one-time large deformation. A group in Sichuan has shown for multiphase composites that low B corresponds to high structural integrity [54]. Brittleness can be connected to several mechanical or tribological properties [55]. We present B values for our materials in Fig. 13.

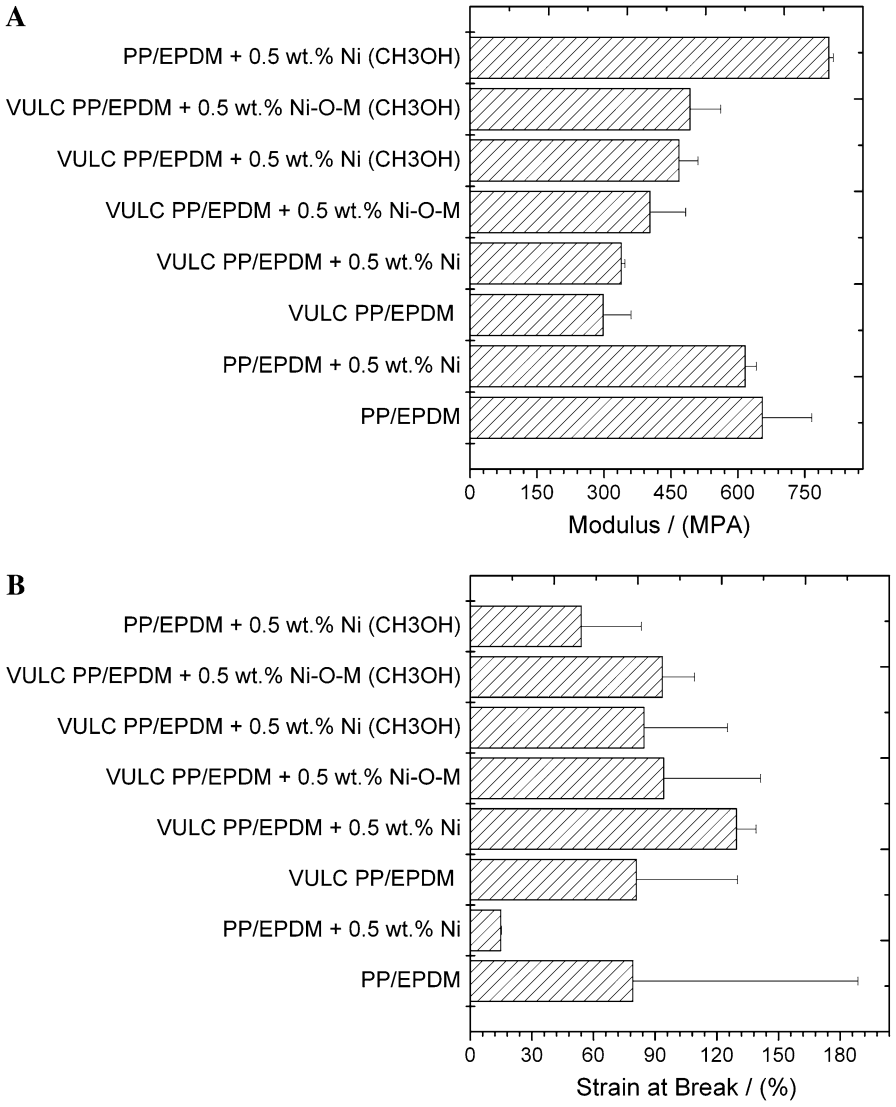

Fig. 12 Young's modulus (**a**) and strain at break (**b**) in tension

We see that brittleness of uncured PP + EPDM increases by a factor of five after addition of 0.5 wt% Ni following Method 1. We have 10^{10}B/(%Pa) = 0.369 for the former and 1.86 for the latter. Clearly, addition of Ni particles to the unvulcanized neat blend increases the brittleness of the system due to lowering cohesion of chains in the polymer matrix. If instead of adding Ni we vulcanize the neat polymer blend, we get in the same units the value 0.444; thus vulcanization also increases *B*, but by a relatively small amount. Apparently crosslinking lowers the chain mobility somewhat.

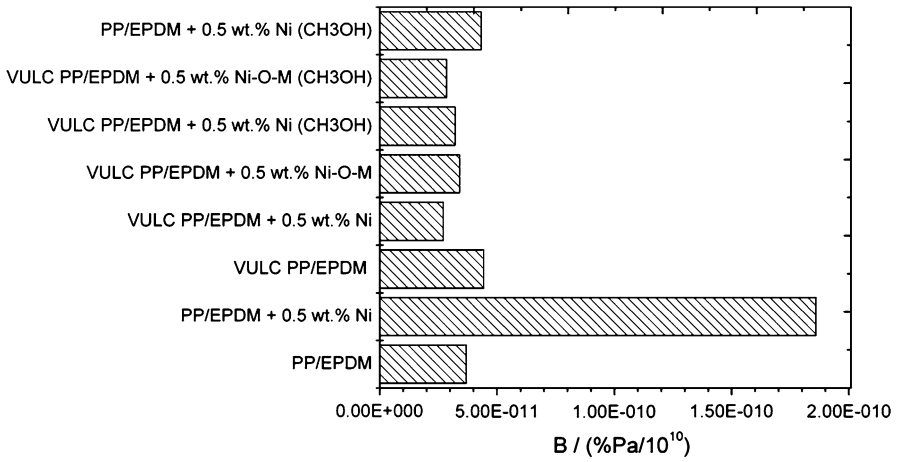

Fig. 13 Brittleness

Consider now the process of *adding Ni combined with* vulcanization and with nickel modification. We thus achieve the lowest value of all, 10^{10}B/(%Pa) = 0.271, that is 27% less than the original unvulcanized blend without nickel. We recall that the same material has the largest elongation at break ϵ_b. Mechanical properties of PBMs are strongly dependent on free volume [2]. Filler particles added can go into existing free volume spaces between chains thus reinforcing the material and resulting in higher values of mechanical properties—as seen in the values of the tensile modulus E and the storage modulus E'. On the other hand, our Ni particles can locally "push aside" some fragments of crosslinked chains—thus creating new free volume pockets as already noted above. It is this second scenario which seems to provide an enhanced capability of the crosslinked chains to extend—reflected in an increase of the elongation at break ϵ_b. Thus, both types of locations of incoming filler particles contribute to lowering the brittleness.

We recall now the results of Khumalo et al. [56]: well-dispersed Boehmite has increased ϵ_b of high density polyethylene (HDPE). Addition of Boehmite clearly lowers brittleness of HDPE since both ϵ_b and E' increase with respect to the neat polymer.

As noted above, mechanical properties of the composites are strongly dependent on the materials composition, the particles dispersion and the interaction (or adhesion) between the filler–matrix interfaces. Another important parameter determining performance of dynamic vulcanized thermoplastic-elastomer-based composites is the crosslink density. Modulus, hardness, tear, tensile strength, creep, and relaxation all depend strongly on the crosslink density n.

We have performed equilibrium swelling measurements in cyclohexane. In principle, n should be independent of the solvent. In practice, minor variations are observed [57]. We have calculated n from swelling results as follows:

$$n = -\left[\ln\left(1 - f_{ps}\right) + f_{ps} + cf_{ps}\right] / \left[V_1\left(f_{ps} - wf_{ps}^{5/3}\right)\right]. \quad (5)$$

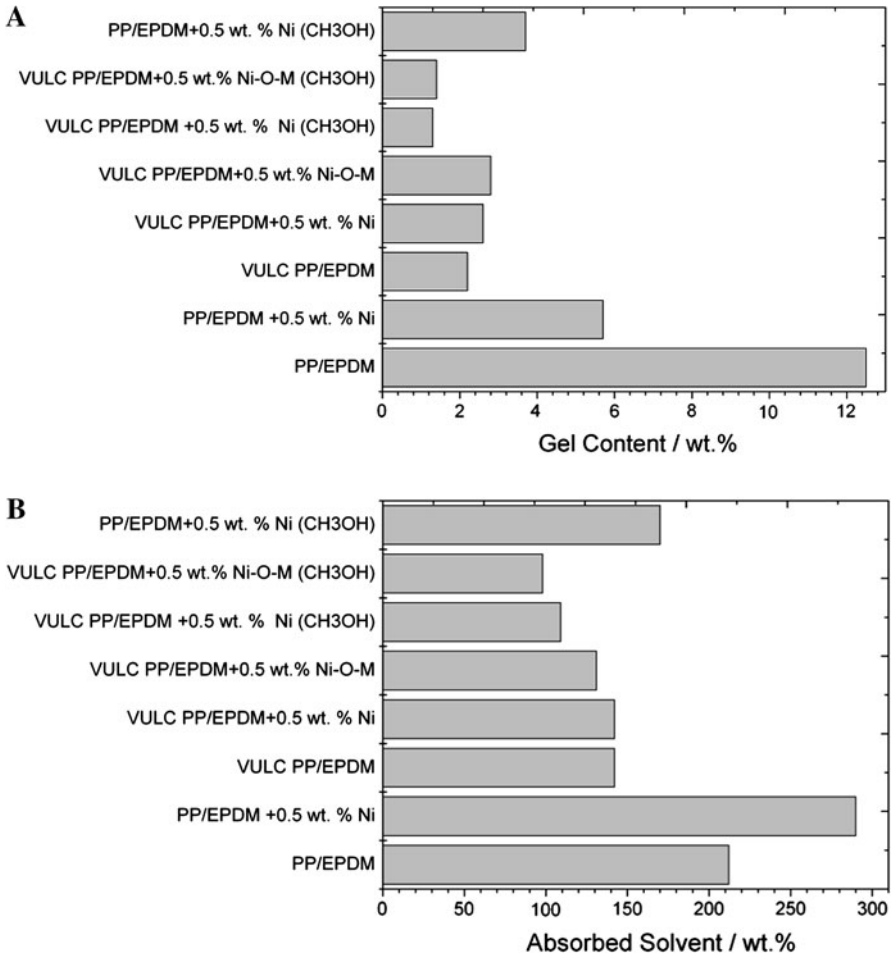

Fig. 14 (**a**, **b**) Gel content and absorbed solvent

Here f_{ps} is the volume fraction of the polymer at swelling equilibrium; clearly in the dry state $f_{ps} = 1$; c the Flory–Huggins–Staverman (polymer + liquid) interaction parameter; V_1 the molar volume of the solvent; w an entropic volume factor $= 2/f$, where f is the functionality. The functionality of a monomer molecule is the number of functional groups which participate in the polymerization. Monomers with functionality greater than two will introduce branching into a polymer, and the degree of polymerization will depend on the average functionality per monomer unit.

We have used $c = 0.420$, a value for PP + cyclohexane, assuming that the presence of EPDM does not significantly affect this value. $V_1 = 108.10$ cm^3 mol^{-1} for cyclohexane; $f = 4$.

The gel content and adsorbed solvent of the samples are shown in Fig. 14.

It can be seen from Fig. 14 that the DCP curing agent exhibits good chemical activity for all vulcanized blends. Almost fully crosslinked composites ($\approx$98.0 wt%) were obtained using 1.0 wt% DCP as a crosslinking agent. The gel content analysis revealed a higher degree ($\approx$99.0 wt%) of crosslinking for the composites from Method 2. A decreased value of the solvent uptake indicates also an increase of crosslink density for the vulcanized samples from Method 2. The gel content and adsorbed solvent amount are related to the crosslinking degree. Both parameters demonstrated significant differences between two sets of the samples from Methods 1 and 2, respectively. All the samples from Method 1 show higher amount of gel content and increased amount of adsorbed solvent. Furthermore, we noticed that, after the addition of nickel particles into PP + EPDM matrix, the amount of the extracted gel decreased from some 12.0 wt% (uncured PP + EPDM) to 6.0 wt% (uncured PP + EPDM + 0.5 wt% Ni) (Fig. 14b). These results indicate that nickel particles act as compatibilization sites. The role of a compatibilizer in a polymer alloy or blend is to improve interfacial adhesion between two immiscible polymers, resulting in the formation of miscible blends. The addition of the compatibilizers results in a decreased domain size of the dispersed phase, stabilization of the dispersed phase during melt mixing, and an improved interfacial adhesion in the solid state. In our PP + EPDM polymers, the nanosized Ni particles provide stabilization energy for compatibilization. Also the intercalation of the polymers with the Ni particles, along with a very high surface area per unit weight of the Ni particles, further helped in compatibilization. The addition of Ni particles also helped to increase the melt viscosity, which further reduced the size of the Ni agglomerates. New multifunctional TPE + 0.5 wt% Ni nanocomposites eliminate oxidation and corrosion problems—while providing much stronger and less brittle materials than neat TPE.

Acknowledgments We appreciate discussions with Olena Astahova, Michael Bratychak, Volodymyr Donchak, and Olena Shyshchak, all at Lvivska Politechnika National University; with Georg Broza and Karl Schulte, Technical University of Hamburg; with Victor Castaño and J. Rogelio Rodriguez, National Autonomous University of Mexico, Queretaro; with Helena Janik, Technical University of Gdansk; with Aglaia Vassilikou-Dova and Ioannis Kalogeras, University of Athens; and also with Tomasz Sterzynski, Poznan University of Technology.

References

1. Friedrich K, Lu Z, Hager AM (1995) Recent advances in polymer composites tribology. Wear 190:139–144
2. Brostow W (2009) Reliability and prediction of long term performance of polymer-based materials. Pure Appl Chem 81:417–420
3. Bobadilla-Sánchez EA, Martínez-Barrera G, Brostow W, Datashvili T (2009) Effects of polyester fibers on gamma irradiation on mechanical properties of polymer concrete containing $CaCO_3$ and silica sand. Express Polym Lett 3:615–620
4. Brostow W (ed) (2000) Performance of plastics. Hanser, Munich/Cincinnati
5. Rabello M (2000) Aditivação de Polimeros. Artliber, São Paulo
6. El-Tayeb NSM, Yousif BF (2007) Evaluation of glass fibre reinforced polyester composite for multi-pass abrasive wear applications. Int J Wear 262:1140–1151
7. Vu YT, Mark JE, Pham LH, Engelhardt M (2001) Clay nanolayer reinforcement of cis-1,4-poly-isoprene and epoxidized natural rubber. J Appl Polym Sci 82:1391–1403

8. Brostow W, Keselman M, Mironi-Harpaz I, Narkis M, Peirce R (2005) Effects of carbon black on tribology of blends of poly(vinylidene fluoride) with irradiated and non-irradiated ultrahigh molecular weight polyethylene. Polymer 46:5058–5064
9. Briscoe BJ, Yao LH, Stolarski TA (1986) The friction and wear of polytetrafluoroethylene poly(ether ether ketone) composites: an initial appraisal of the optimum composition. Wear 108:357–374
10. Carrión FJ, Arribas A, Bermúdez MD, Guillamon A (2008) Physical and tribological properties of a new polycarbonate-organoclay nanocomposite. Eur Polym J 44:968–977
11. Gatos KG, Thomann R, Karger-Kocsis J (2004) Characteristics of ethylene propylene diene monomer rubber/organoclay nanocomposites resulting from different processing conditions and formulations. Polym Int 53:1191–1197
12. Chow WS, Mohd Ishar ZA, Karger-Kocsis J (2005) An atomic force microscopy study on the blend morphology and clay dispersion in polyamide-6 polypropylene/organoclay system. J Polym Sci B 43:1198–1204
13. Karger-Kocsis J, Shang PP, Mohd Ishak ZA, Rösch M (2007) Melting and crystallization of in situ polymerized cyclic butylene terephthalates with and without organoclay: a modulate DSC study. Express Polym Lett 1:60–68
14. Gatos KG, Kameo K, Karger-Kocsis J (2007) On the friction and sliding wear of rubber/layered silicate nanocomposites. Express Polym Lett 1:27–31
15. Pegoretti A, Dorigato A, Penati A (2007) Tensile mechanical response of polyethylene-clay nanocomposites. Express Polym Lett 1:123–131
16. Varghese S, Karger-Kocsis J, Gatos KG (2003) Melt compounded epoxidized natural rubber/layered silica nanocomposites: structure–properties relationships. Polymer 44:3977–3983
17. Wang K, Zhao P, Yang S, Liang S, Zhang Q, Du R, Fu Q, Yu Z, Chen E (2002) Unique clay orientation in the injection-molded bar of isotactic polypropylene/clay nanocomposite. Polymer 47:7103–7110
18. Brostow W, Pietkiewicz D, Wisner SR (2007) Polymer tribology in safety medical devices: retractable syringes. Adv Polym Technol 26:56–64
19. Brostow W, Bujard B, Cassidy PE, Venumbaka S (2004) Epoxy + fluoropolymer systems: nanoscale surface organization and scratch resistance. Int J Polym Mater 53:1045–1050
20. Brostow W, Datashvili T (2007) Miscibility and thermal properties of blends of melamine–formaldehyde resin with low density polyethylene. Mater Res Innovat 11:127–130
21. Kalogeras M, Roussos M, Christakis I, Spanoudaki A, Pietkiewicz D, Brostow W, Vassilikou-Dova A (2005) Dielectric properties of cured epoxy resin + poly (ethylene oxide) blends. J Non-Cryst Solids 351:2728–2734
22. Nogales A, Broza G, Roslaniec Z, Schulte K, Sics I, Hsiao BS, Sanz A, Garcia-Gutierrez MC, Rueda DR, Domingo C, Ezquerra TA (2004) Low percolation threshold in nanocomposites based on oxidized single wall carbon nanotubes and poly(butylene terephthalate). Macromolecules 37:7669–7673
23. dos Santos DS Jr, Goulet PJG, Pieczonka NPW, Oliveira ON Jr, Aroca JR (2004) Gold nanoparticle embedded, self-sustained chitosan films as substrates for surface-enhanced Raman scattering. Langmuir 20:10273–10277
24. Koo JH (2006) Polymer nanocomposites: processing, characterization, and applications. McGraw-Hill, New York, NY, pp 19–26
25. Giraldo LF, Brostow W, Devaux E, López BL, Pérez LD, León D (2008) Scratch and wear resistance of polyamide 6 reinforced with multiwall carbon nanotubes. J Nanosci Nanotechnol 8:3176–3183
26. Luo ZP, Koo JH (2008) Quantification of the layer dispersion degree in polymer layered silicate nanocomposites by transmission electron microscopy. Polymer 49:1841–1852
27. Broza G, Schulte K (2008) Melt processing and filler/matrix interphase in carbon nanotube reinforced poly(ether-ester) thermoplastic elastomer. Polym Eng Sci 48:2033
28. Brostow W, Chonkaew W, Datashvili T, Menard KP (2009) Tribological properties of epoxy + silica hybrid materials. J Nanosci Nanotechnol 9:1916–1922
29. Blanksi R, Koo JH, Ruth P, Nguyen H, Pittman C, Phillips S (2004) Polymer nanostructured materials for solid rocket motor insulation—ablation performance. In: Proceedings of the 52nd JANNAF propulsion meeting (CPIAC'04), Columbia, MD
30. Naderi G, Lafleur PG, Dubois C (2008) The influence of matrix viscosity and composition on the morphology, rheology, and mechanical properties of thermoplastic elastomer nanocomposites based on EPDM/PP. Polym Compos 29:1301–1309
31. Ho WK, Koo JH, Ezekoye OA (2010) Thermoplastic polyurethane elastomer nanocomposites: morphology, thermophysical, and flammability properties. J Nanomater doi:10.1155/2010/583234

32. Foks J, Janik H (1989) Microscopic studies of segmented urethanes with different hard segment content. Polym Eng Sci 29:113–119
33. Rutkowska M, Krasowska K, Heimowska A, Steinka I, Janik H (2002) Degradation of polyurethanes in sea water. Polym Degrad Stabil 76:233–239
34. Janik H, Pałys B, Petrovic ZS (2003) Multiphase-separated polyurethanes studied by micro-Raman spectroscopy. Macromol Rapid Commun 24:265–268
35. Brostow W, Buchman A, Buchman E, Olea-Mejía O (2008) Micro hybrids of metal powder incorporated in polymeric matrices: friction, mechanical behavior, and microstructure. Polym Eng Sci 49:1977–1981
36. Brostow W, Simões R (2005) Tribological and mechanical behavior of metals and polymers simulated by molecular dynamics. J Mater Educ 27:19–28
37. Brostow W, Gorman BP, Olea-Mejia O (2007) Focused ion beam milling and scanning electron microscopy characterization of metal + polymer hybrids. Mater Lett 61:1333–1336
38. Coran AY (1987) Thermoplastic rubber-plastic blends. In: Bhowmick AK, Stephens HL (eds) Handbook of elastomer-new development and technology. Marcel Dekker, New York, pp 249–313
39. Brostow W, Datashvili T, Strate GW, Lohse DJ (2009) Ethylene-propylene-diene monomer elastomers. In: Mark JE (ed) Polymer data handbook, 2nd edn. Oxford University Press, Oxford, pp 155–162
40. Brostow W, Datashvili T, Hackenberg KP (2010) Effect of different types of peroxides on properties of vulcanized EPDM + PP blends. Polym Compos 31:1678–1691
41. Brostow W, Datashvili T, Geodakyan J, Lou J (2011) Thermal & mechanical properties of EPDM/PP + thermal shock-resistant ceramic composites. J Mater Sci 46:2445–2455
42. Song P, Wen D, Guo ZX, Korakianitis T (2008) Oxidation investigation of nickel nanoparticles. Phys Chem Chem Phys 10:5057–5065
43. Karmhag R, Niklasson G, Nygren M (2001) Oxidation kinetics of nickel nanoparticles. J Appl Phys 89:3012–3017
44. Niklasson G, Karmhag R (2003) Oxidation kinetics of metallic nanoparticles. Surf Sci 532–535:324–327
45. Menard KP (2000) Thermal transitions and their measurement. In: Brostow W (ed) Performance of plastics, Chap. 8. Hanser, Munich/Cincinnati
46. Lucas EF, Soares BG, Monteiro E (2001) Caracterização de Polímeros. e-papers, Rio de Janeiro
47. Gedde UW (2001) Polymer physics. Springer, Dordrecht/Boston
48. Mandelkern L, Alamo RG (2007) Thermodynamic quantities governing melting. In: Mark JE (ed) Physical properties of polymers handbook, 2nd edn. Springer, New York, pp 165–186
49. Hedenqvist MS, Gedde UW (1999) Parameters affecting the determination of transport kinetics data in highly swelling polymers above T_g. Polymer 40:2381–2393
50. Yoldas BE (1975) Alumina sol preparation from alkoxides. Ceram Bull 54:289–290
51. Kopczynska A, Ehrenstein GW (2007) Polymeric surfaces and their true surface tension in solids and melts. J Mater Educ 29:325–340
52. Brostow W, Deshpande S, Pietkiewicz D, Wisner SR (2009) Accuracy in locating glass transitions: aging and gamma sterilization of vulcanized thermoplastic elastomers. e-Polymers 109
53. Brostow W, Hagg Lobland HE, Narkis M (2006) Sliding wear, viscoelasticity, and brittleness of polymers. J Mater Res 21:2422–2428
54. Shen J, Wang M, Li J, Guo S, Xu S, Zhang Y, Li T, Wen M (2009) Simulation of mechanical properties of multilayered propylene–ethylene copolymer/ethylene 1-octene copolymer composites by equivalent box model and its experimental verification. Eur Polym J 45:3269–3281
55. Brostow W, Hagg Lobland HE, Narkis M (2011) The concept of materials brittleness and its applications. Polym Bull 59. doi:10.1007/s00289-011-0573-1
56. Khumalo VM, Karger-Kocsis J, Thomann R (2011) Polyethylene/synthetic boehmite alumina nanocomposites: structure, mechanical, and perforation impact properties. J Mater Sci 46:422–428
57. Flory PJ (1953) Principles of polymer chemistry. Cornell University Press, Ithaca, NY